Materials and Design 60 (2014) 678–684

Contents lists available at ScienceDirect

Materials and Design

journal homepage: www.elsevier.com/locate/matdes

Effect of heat input on microstructure and mechanical properties of dissimilar joints between super duplex stainless steel and high strength low alloy steel

M. Sadeghian, M. Shamanian *, A. Shafyei

Department of Materials Engineering, Isfahan University of Technology, Isfahan 8415683111, Iran

ARTICLE INFO

Article history:
Received 14 January 2014
Accepted 24 March 2014
Available online 13 April 2014

Keywords:
Dissimilar welding
Super duplex stainless steels
High strength low alloy steel
Heat input
Microstructure
Mechanical properties

ABSTRACT

In the present study, microstructure and mechanical properties of UNS S32750 super duplex stainless steel (SDSS)/API X-65 high strength low alloy steel (HSLA) dissimilar joint were investigated. For this purpose, gas tungsten arc welding (GTAW) was used in two different heat inputs: 0.506 and 0.86 kJ/mm. The microstructures investigation with optical microscope, scanning electron microscope and X-ray diffraction showed that an increase in heat input led to a decrease in ferrite percentage, and that detrimental phases were not present. It also indicated that in heat affected zone of HSLA base metal in low heat input, bainite and ferrite phases were created; but in high heat input, perlite and ferrite phases were created. The results of impact tests revealed that the specimen with low heat input exhibited brittle fracture and that with high heat input had a higher strength than the base metals.

1. Introduction

Duplex (DSS) and super duplex (SDSS) stainless steels consist of approximately equal amounts of austenite and ferrite, which combine the attractive properties of austenitic and ferritic stainless steels such as high strength, highly resistant to chloride stress corrosion cracking, and have excellent pitting and crevice corrosion resistance [1,2].

Due to their corrosion resistance and improved mechanical properties, these steels are extensively used in petrochemical and chemical industries as pipes, pumps, pressure vessels, separators and heat exchangers [3–5]. Moreover, SDSS are widely used in offshore equipment in contact with aggressive chemicals such as H_2S, CO_2, CN^- and Cl^- [6].

The best properties of DSS and SDSS are obtained with the ferrite–austenite ratio close to 50:50 [1,6]; and detrimental phases such as sigma (σ), chi (χ), secondary austenite (γ_2), chromium carbides and nitrides, which affect the corrosion resistance and toughness in the SDSSs are not present [7].

In welding operations, very low heat inputs lead to high ferrite contents and intense chromium nitride precipitation. On the other hand, high heat inputs and/or long exposure to temperatures in the 600–1000 °C range may cause precipitation of brittle intermetallic phases such as σ or χ [1,7]. In general, welding specifications must be designed to obtain phase proportions (ferrite/austenite ratio) near 1:1 and to avoid σ and Cr_2N precipitation by controlling and limiting the heat input to 0.5–2.0 kJ/mm for DSSs [8] and 0.5–1.5 kJ/mm for SDSSs [9].

With the growing application of new materials and higher demands for such materials, a great need arises for the component or structure of dissimilar materials [10]. Dissimilar joint of SDSS and high strength low alloy steel (HSLA) pipes have been widely employed in the oil and gas industry. Welding dissimilar materials is generally more challenging than welding similar ones because of differences in the chemical, physical and mechanical properties of the base metals welded [7,10]. Therefore, it is critical to understand the heat input–property relationships in joints between SDSS and HSLA. Although certain amounts of research work have been carried out on the microstructure and properties of dissimilar joints between SDSS and HSLA [11–14], no systematic build-up on the effects of heat input on a microstructure and mechanical properties of dissimilar joints between DSS and HSLA has been proposed. Gas tungsten arc welding (GTAW) is the most widely employed joining process in engineering industries, especially in those dealing with structural and piping applications [15]. Therefore, the aim of this study is to investigate the effect of heat input on the microstructure and mechanical properties of dissimilar joints between a SDSS and a HSLA by employing GTAW process.

* Corresponding author. Tel./fax: +98 311 3915737.
E-mail address: shamanian@cc.iut.ac.ir (M. Shamanian).

http://dx.doi.org/10.1016/j.matdes.2014.03.057
0261-3069/

2. Experimental procedure

The materials employed in this study were API X-65steel and UNS S32750 SDSS, both supplied in seamless pipe shapes with an internal diameter of 508 mm (20 in.) and a nominal thickness of 4 mm (0.15 in.). The GTAW process with direct electrode and negative polarity (GTAW–DCEN) was chosen for welding because of its flexibility in field applications, which is a necessity in the petrochemical industry [12]. A 70 degree single V groove edge with a root-face gap of 2 mm was employed before welding. Also, an ER25.10.4.L welding rod consumable in two passes was used to join UNS S32750 SDSS grade to API X-65 HSLA grade. The compositions of base metals and filler metal are shown in Table 1. The weld beads were produced in two different heat inputs. Table 2 shows the welding parameters.

In order to investigate the microstructural changes related to welding process, samples were taken from the base metals and the welds. Specimens for the metallographic examinations were prepared using conventional metallographic methods with final 3 μm diamond slurry disc polishing. The etching of API X-65 was carried out using 2% Nital + 4% Picral solution, and an electrolytic etching in 20% Sodium hydroxide (3 V for 5–10 s) was employed for the UNS S32750 and weld metals [16]. This etchant solution is useful for the determination of sigma and chi phases in DSSs (ASTM: A 923-08). The microstructural features then were examined in high-resolution optical microscope (OM) and scanning electron microscope (SEM).

X-ray diffraction (XRD) was carried out on specimens. X-ray diffractory was done using Philips X'PERT MPD diffractometer with Cu Kα ($\lambda = 0.154$ nm). Other measured parameters were: voltage 20 kV, current 30 mA, angular interval (2θ) 20–110°, angular step 0.02° and counting time 3 s.

Ferrite number measurements were also carried out using Feritscope® FMP30 calibrated with secondary standards according to ANSI/AWS A4.2-91 [17].

Microhardness measurements were made across the base materials, heat affected zones and weld metal, and were investigated at 100 g loading in 10 s.

Samples of reduced Charpy size (2.5 mm) were cut from the weld joint, and were machined in accordance with the ASTM:E23-12c standard. Impact tests were performed at −20 °C. Macroscopic and microscopic examinations of the fractured specimens were carried out in a stereo zoom microscope and SEM, respectively.

3. Result and discussion

3.1. Microstructures

3.1.1. Base metal and weld metal microstructures

The microstructures of UNS S32750 SDSS and API X-65 steel base materials are shown in Figs. 1(a and b), respectively. UNS S32750 SDSS base material has an elongated grain structure, which is typical in rolled products. This base metal contains 46% ferrite (±2.5%). The HSLA base material has a near-equiaxed grain structure comprised of predominant ferrite matrix with small amounts of pearlite.

The main goal of metallographic examinations was determining the general microstructure of the weld metal and heat affected zones (HAZ) [18]. So, in the metallographic observations, the samples were searched for secondary austenite and intermetallic precipitations. The width of HAZ was also measured, and special attention was paid to seeking any solidification cracking in the weld structure.

General structures of the weld zone in the joints were similar. During solidification of super duplex weld metal, ferrite is the only phase which is solidified. Further cooling in solid state initiates the formation of austenite phase at the delta-ferrite grain boundaries [7]. As can be seen in Fig. 2, austenite and ferrite phases with a dendritic microstructure are caused by fast cooling rates [18]. Austenite and ferrite were distributed uniformly in the weld metal and no detrimental secondary or intermetallic phase was present. Fig. 3 shows the X-ray diffractograms of weld metals. It is clear that detriment phases are not detected by X-ray diffraction.

The volume fraction of ferrite in weld metals were 44% and 38%. For most industrial applications, austenite contents lower than 25% are unacceptable. Also, for welding and piping inspection, the minimum austenite content should be 30% in the last bead and root passes as a necessary value in order to accept the joint weld [6]. The results indicate that the austenite content of weld metals is accepted, and increases as the heat input increases.

The balance of austenite and ferrite in the weld metal can be controlled in two different ways: adjusting the chemical composition of the weld metal and controlling the thermal cycle of the welding process. Chemical composition can be controlled by selecting the suitable filler metal, which should promote the austenite phase formation in solid state with elements such as nickel and nitrogen [12]. The large amount of austenite in the weld metals is attributed to the chemical composition of filler metals – mainly the Ni element content [11] and the migration of carbon element from HSLA to weld metal. The welding thermal cycles also can be utilized to obtain a favorable equilibrium between austenite and ferrite phases. However, low cooling rates (high heat inputs) may lead to the precipitation of intermetallic phases, and must be avoided [12]. When chemical composition is fixed, the only way to control the austenite/ferrite balance is to control the heat input. The cooling rate is reduced by increasing the heat input [19]. As the heat input increases, the weld metal stays longer in high temperature ranges and more ferrite is transformed into austenite. In this study, the heat input was limited to 0.5–0.86 kJ/mm; so, the precipitation of brittle intermetallic phases was not possible.

3.1.2. Heat affected zone microstructures

Evolution of the HAZ microstructure in welding is more complicated, and depends upon more factors including the original base

Table 1
Chemical compositions of base metals and filler metal (wt.%).

Element	C	Mn	Si	Cr	Ni	Mo	N	Fe	Cr_{eq}	Ni_{eq}	PREN
UNS S32750	0.03	0.82	0.93	25.7	6.3	3.4	0.23	Bal.	29.1	11.95	43.82
API X65	0.26	1.30	0.411	0.016	<0.030	0.049	–	Bal.	0.064	9.2	0.174
Filler metal	0.03	0.73	0.94	25.9	9.2	4.2	0.22	Bal.	30.1	14.65	46.36

Table 2
The welding parameters and the heat inputs.

Sample	Current (A)	Volt (V)	Length (mm)	Time (s)	Speed (mm s^{-1})	Heat input (kJ mm^{-1})
1	100	15	160	90	1.8	0.506
2	120	16.75	140	100	1.4	0.861

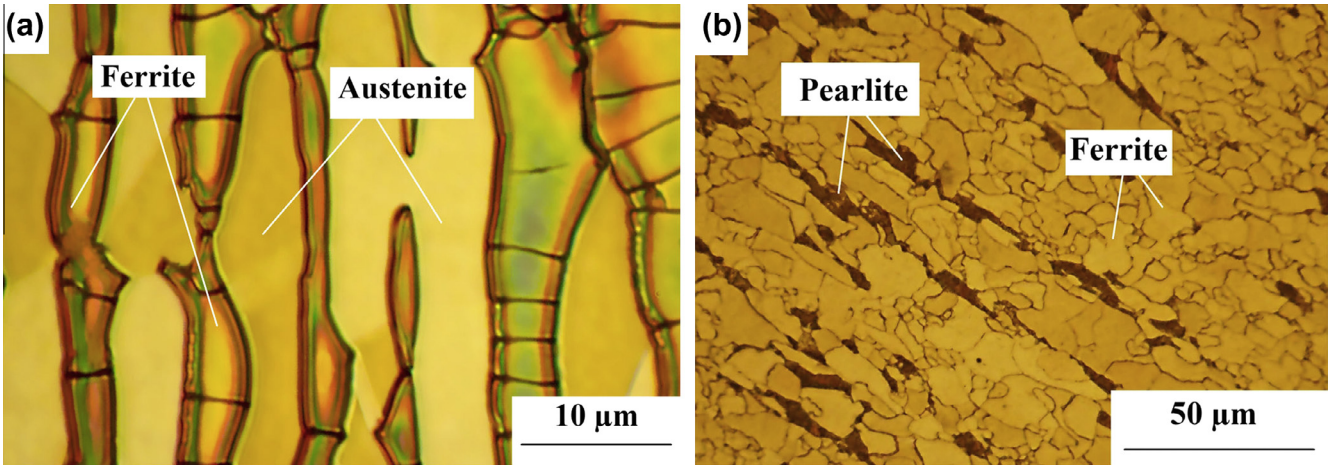

Fig. 1. Microstructure of base materials: (a) UNS S32750 SDSS (b) API X-65 steel.

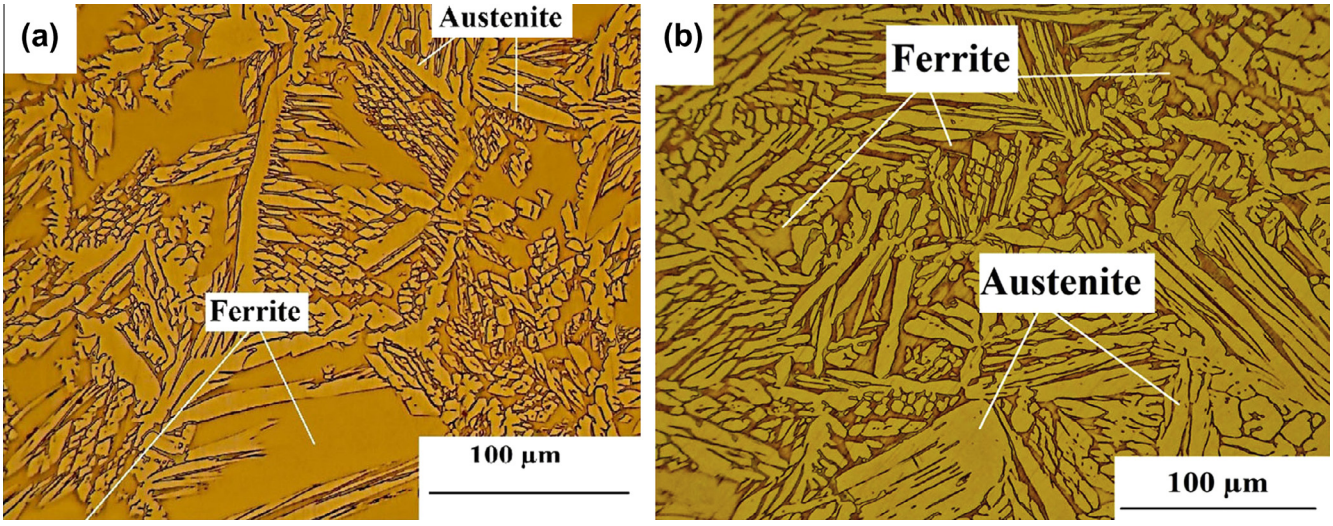

Fig. 2. Microstructure of the welded metals (a) sample 1, and (b) sample 2.

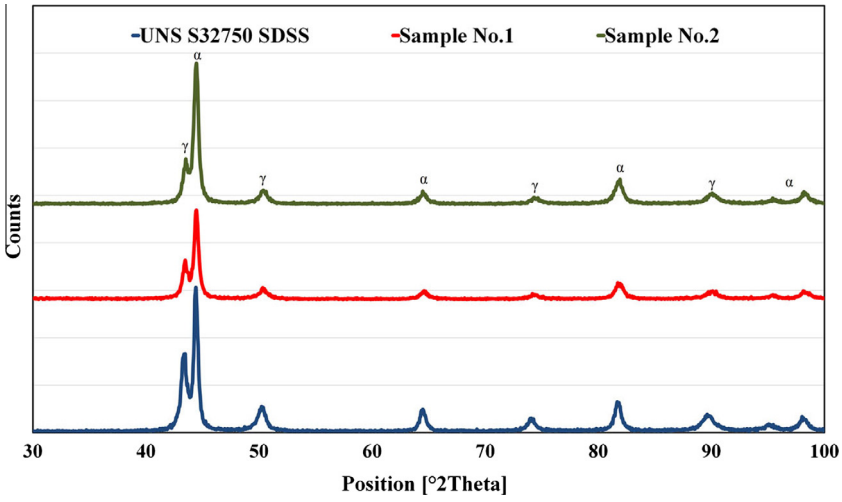

Fig. 3. X-ray diffractograms of 32750 SDSS and weld metals.

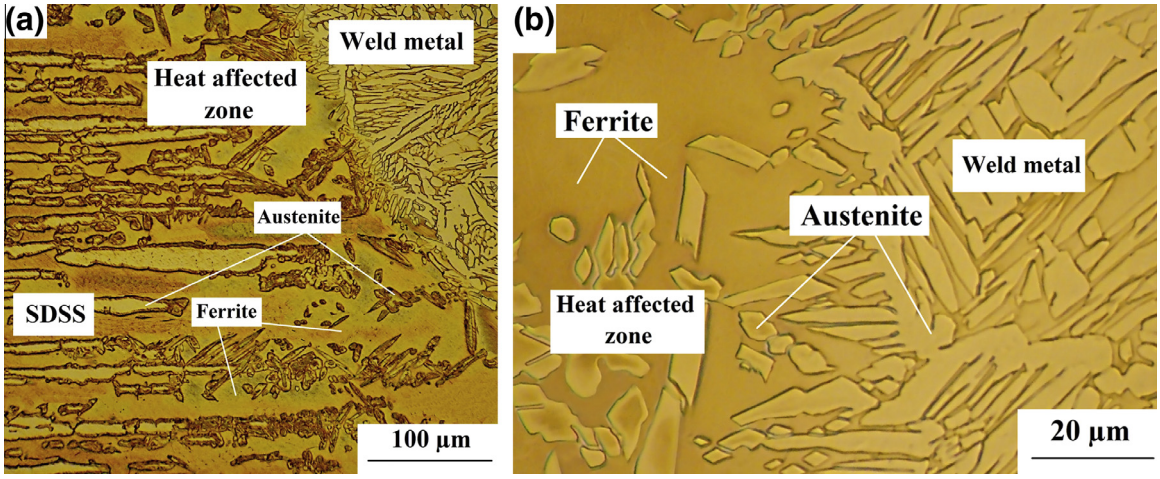

Fig. 4. Microstructure of heat affected zone. SDSS side. (a) Low magnify and (b) high magnify.

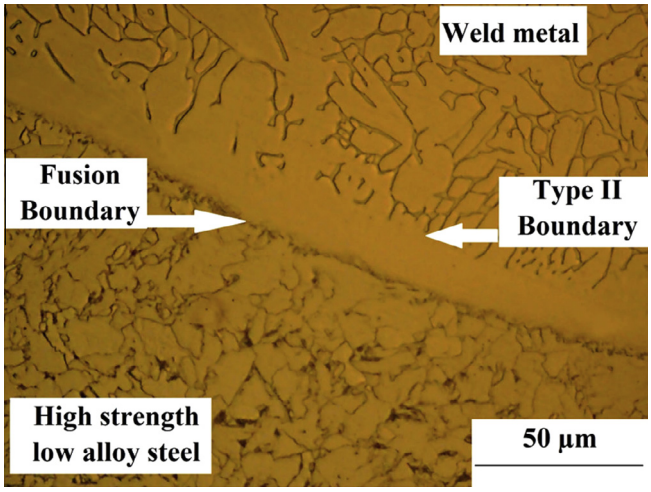

Fig. 5. Microstructure of heat affected zone. HSLA side.

metals' microstructure, peak temperature experienced by the HAZ region, presence time at peak temperature, and the heating and cooling rates [20].

The HAZ on the SDSS side is very narrow, about 200 µm in width (Fig. 4a). With higher cooling rates which occur in welding [12,18], it is possible to observe that austenite reformation is suppressed, and higher ferrite contents are present in the HAZ (Fig. 4b).

The HAZ on the HSLA side is shown in Fig. 5. As can be seen, a type II boundary characteristic of dissimilar joints was observed close to the fusion boundary. The development of such boundary has been attributed to the differences in the crystal structure between the materials being joined, and has been addressed in the literature for dissimilar fusion welded joints between austenitic and ferritic steels [15].

The HAZ on the HSLA side shows solid phase transformations typical of the alloy when it is submitted to thermal cycles as shown in Fig. 6. Due to rapid cooling, the microstructure of HAZ on sample 1 is more notable where the upper bainite (UB) which has a feathery appearance can be distinguished. However, the polygonal ferrite is obtained when the cooling rate is slow as presented in the HAZ of sample 2. The results of this study are in agreement with those obtained by Bravo et al. [12].

3.2. Mechanical properties

3.2.1. Microhardness profile

Microhardness profile across the joints interface are shown in Fig. 7. The trend of microhardness change is almost the same in all welded joints. Obviously, the hardness value of the weld metal

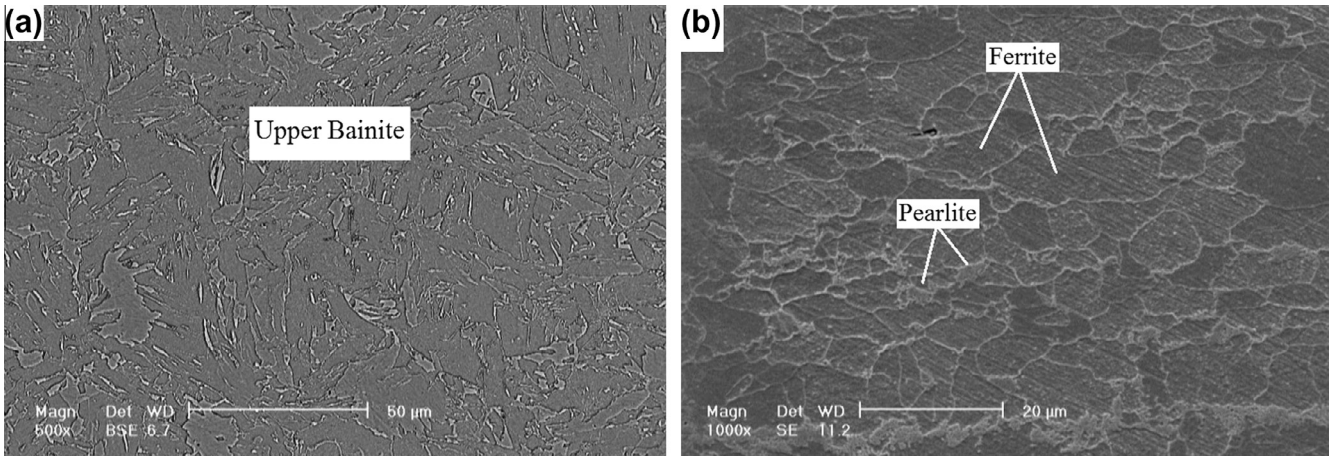

Fig. 6. SEM micrographs of Heat affected zone. HSLA side. (a) Sample 1, and (b) sample 2.

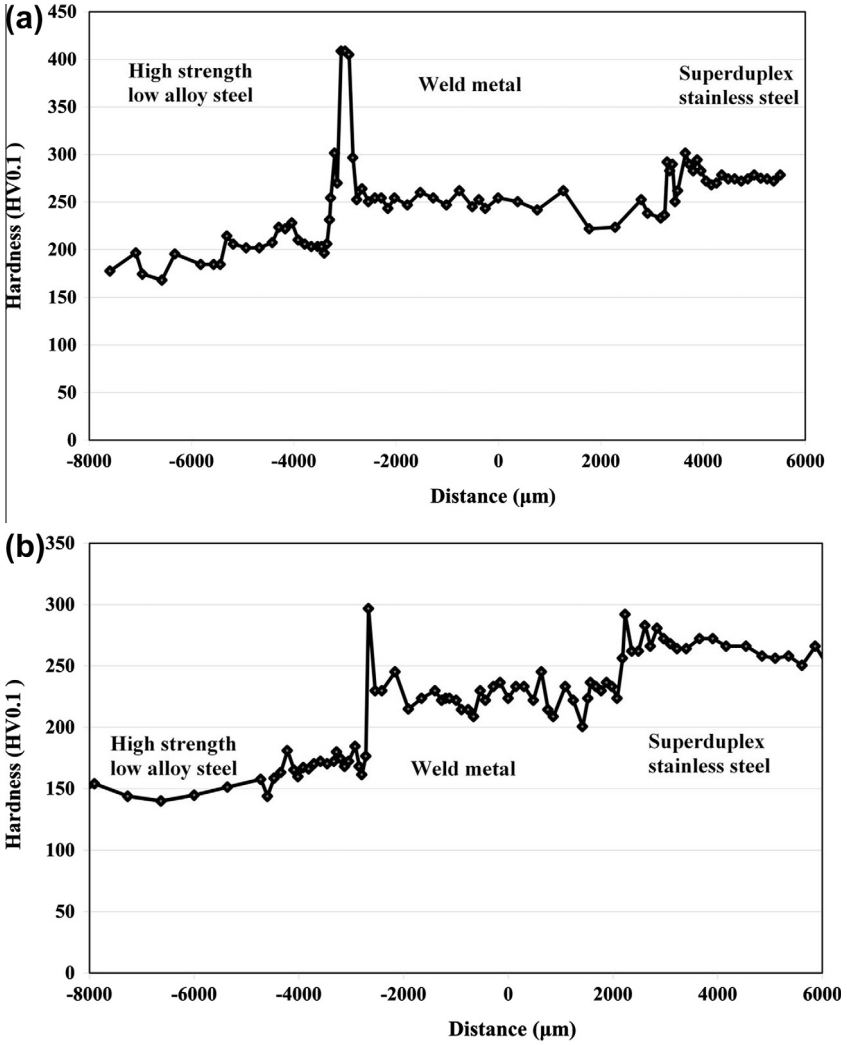

Fig. 7. Microhardness profiles of the dissimilar metal welding. (a) Sample 1, and (b) sample 2.

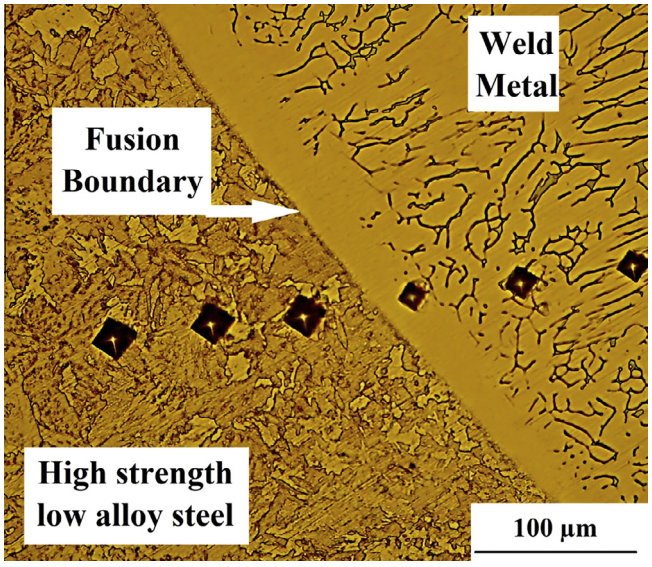

Fig. 8. Hardness variation across the HSLA–WM interface.

is higher than that of the HSLA base metal and the HAZ of HSLA, which can be attributed to the differences in chemical properties.

Table 3
The average of Charpy V-notch impact energy for weld metals.

	Impact strength (j)	Fracture type
SDSS base metal	34	Ductile
HSLA base metal	34	Ductile
Sample 1	32	Ductile/brittle
Sample 2	42	Ductile

The difference in microhardness of HAZ between different weldments can be attributed to the differences in the morphology and distribution of microconstituents – such as martensite or carbides – in the resultant weld metals (Fig. 6). Furthermore, the higher amounts of hardness observed in the narrow zone between the fusion boundary and type II boundary in all weldments confirm the formation of harder microconstituents in this region owing to the carbon migration from the HSLA side. This is depicted in the optical micrograph of Fig. 8 [15]. Variation of microhardness in HAZ of SDSS is also evident in Fig. 4. This can be attributed to the differences in the austenite-ferrite ratio and variations of Cr content in HAZ of SDSS (Fig. 4).

3.2.2. Impact toughness

The impact strength values of the base materials and weld metals tested at −20 °C are presented in Table 3. The data show that

sample 1 exhibited the lower impact strength due to the formation of brittle phases at low heat input (Figs. 6a and 7a). The macroscopic examination of fractured specimen revealed that the crack had a propagation toward HSLA base metal, especially at the HAZ zone (Fig. 9a). It means that the weakest part of the joints is in HSLA base metal.

The impact strength of sample 2, which is associated with high welding heat input is higher than that of both base metals. Sample 2 has a greater heat input compared to sample 1, which results in a slower cooling rate. The ferrite–austenite transformation in this region occurs partially during solidification with the action of weld thermal cycles because there is sufficient time for the diffusion of alloying element chromium throughout the ferrite phase [7,11]. As a result, the ferrite-to-austenite transformation ratio decreases as a function of increased heat input, and more austenite phase is generated in weld metal No. 2 during welding. In the case of sample 2, the fracture propagation was in a straight path confined within the weld metal (Fig. 9b).

The fracture surfaces of base metals and samples were also evaluated by SEM, and the results are shown in Fig. 10. The base metals revealed ductile dimple fracture (Fig. 10a and b). In the case of sample 1, they exhibited a mixed cleavage-type showing a

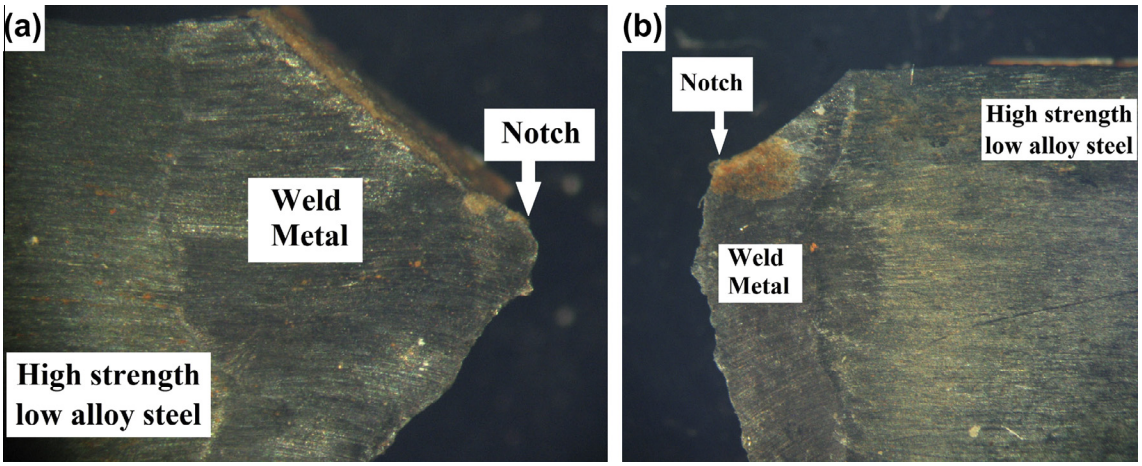

Fig. 9. Macroscopic examination of fractured specimen. (a) Sample 1, and (b) sample 2.

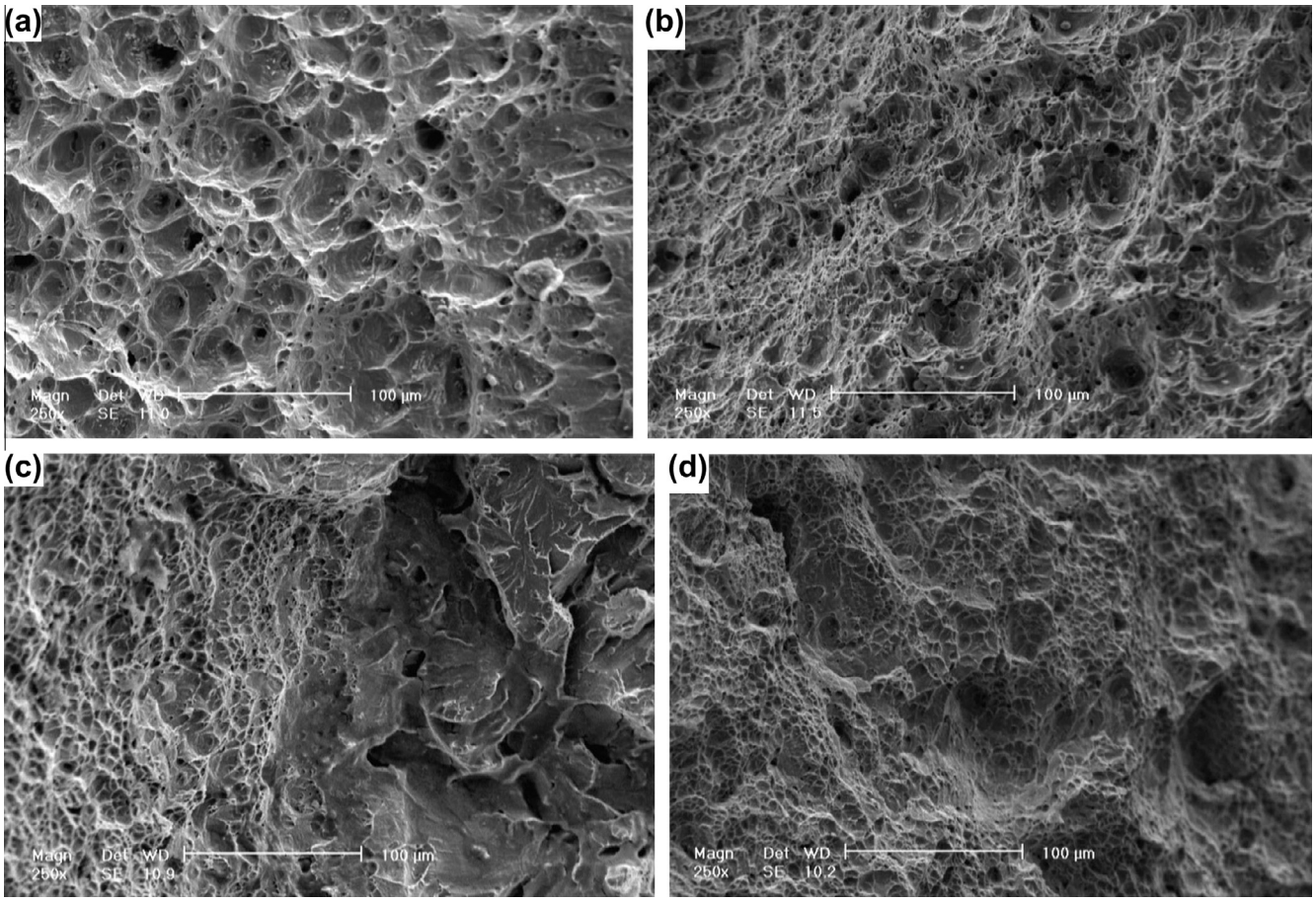

Fig. 10. SEM fractographs of fractured Charpy impact specimens: (a) 32750 SDSS, (b) API X-65 HSLA, (c) Sample 1, and (d) sample 2.

relatively flat surface and ductile fracture (Fig. 10c), which might be attributed to the formation of the brittle phase in HAZ of HSLA side. Test sample 2 (Fig. 10d) an exhibited entirely ductile fracture, attributed to the microstructure of weldment.

4. Conclusions

The investigation of welding between UNS S32750 SDSS and API X-65HSLA by GTAW at different heat input reach the following conclusions:

- The microstructure of weld metals consists of austenite and ferrite, and an increase in heat input leads to a decrease in ferrite content. Detrimental phases are not observed in the current case through analysis of XRD.
- The HAZ of the API X-65 shows different transformations. Due to thermal cycles, a rapid cooling evolved, which is the case of upper bainite phase. However, the polygonal ferrite and perlite with heterogenic distribution are obtained when the cooling rate is slow.
- The microhardness was increased in both welds along the HSLA/weld metal fusion boundary, especially in the sample with the high cooling rate due to the formation of non-equilibrium phases.
- The impact toughness of samples tested at −20 °C revealed that the impact strength of the sample with low heat input was lower than base metals in case the impact strength of the sample with high heat input was higher than base metals.
- Based on the present work, it is summarized that GTAW with filler metal ER25.10.4.L and applied heat input at 0.506 kJ/mm is not the suitable welding procedure for dissimilar metals joining between UNS S32750 SDSS and API X-65HSLA.

References

[1] Muthupandi V, BalaSrinivasan P, Seshadri SK, Sundaresan S. Effect of weld metal chemistry and heat input on the structure and properties of duplex stainless steels. Mater Sci Eng A 2003;358:9–16.
[2] Tan H, Jiang Y, Deng B, Sun T, Xu J, Li J. Effect of annealing temperature on the pitting corrosion resistance of super duplex stainless steel UNS S32750. Mater Charact 2009;60:1049–54.
[3] El-Yazgi AA, Hardie D. Stress corrosion cracking of duplex and super duplex stainless steels in sour environments. Corros Sci 1998;40:909–30.
[4] Cui ZD, Wu SL, Zhu SL, Yang XJ. Study on corrosion properties of pipelines in simulated produced water saturated with supercritical CO_2. Appl Surf Sci 2006;252:2368–74.
[5] Smith L. A guideline to the successful use of duplex stainless steels for flowlines. Stainless Steel World, Duplex America 2000 Conf – KCL Publishing BV, DA2-102: 1–16.
[6] Tavares SSM, Pardal JM, Lima LD, Bastos IN, Nascimento AM, Souza JA. Characterization of microstructure, chemical composition, corrosion resistance and toughness of a multipass weld joint of super duplex stainless steel UNS S32750. Mater Charact 2007;58:610–6.
[7] Kotecki DJ, Lippold JC. Welding metallurgy and weldability of stainless steels. Hoboken, New Jersey: John Wiley; 2005.
[8] Practical guidelines for the fabrication of duplex stainless steels. London: International Molybdenum Association; 1999.
[9] Sandvik SAF 2507. <http://www.smt.sandvik.com>. The date accessed: 02.01.14.
[10] Kacar R, Baylan O. An investigation of microstructure/property relationships in dissimilar welds between martensitic and austenitic stainless steels. Mater Des 2004;25:317–29.
[11] Wang S, Ma Q, Li Y. Characterization of microstructure, mechanical properties and corrosion resistance of dissimilar welded joint between 2205 duplex stainless steel and 16MnR. Mater Des 2011;32:831–7.
[12] Bravo IM, Zepeda CM, Hernandez AA, Piedras ER. Dissimilar welding of super duplex stainless steel/HSLA steel for offshore applications joined by GTAW. Eng 2010;2:520–8.
[13] Xiaoyan W, Lei Z, Xianren K, Minxu L. Microstructure and galvanic corrosion of dissimilar weldment between duplex stainless steel UNS 31803 and X80 steel. In: ASME 28th international conference on ocean, offshore and arctic engineering (OMAE2009), Honolulu, Hawaii, USA; May 31–June 5, 2009.
[14] Barnhouse EJ, Lippold JC. Microstructure/property relationships in dissimilar welds between duplex stainless steels and carbon steels. W J 1998;77:477–87.
[15] Bala Srinivasan P, Muthupandi V, Dietzel W, Sivan V. An assessment of impact strength and corrosion behaviour of shielded metal arc welded dissimilar weldments between UNS 31803 and IS 2062 steels. Mater Des 2006;27:182–91.
[16] ASM Handbook, Metallography and Microstructures. vol. 9. Ohio: ASM International, Materials Park; 2004.
[17] ANSI/AWS A4.2. Standard procedures for calibrating magnetic instruments to measure the delta ferrite content of austenitic and duplex ferritic–austenitic stainless steel weld metal. PA: ANSI/AWS Standard; 1997.
[18] Labanowski J. Mechanical properties and corrosion resistance of dissimilar stainless steel welds. Arch Mater Sci Eng 2007;28:27–33.
[19] Kou Sindo. Welding metallurgy. 2nd ed. Hoboken, New Jersey: John Wiley & Sons, Inc; 2003.
[20] Nelson DE, Baeslack WA, Lippold JC. Characterization of the weld structure in a duplex stainless steel using color metallography. Metallography 1985;18:215–25.